Dy^{3+} single ion magnet in the extended inorganic solid $Ca(Y,Dy)AlO_4$

Pavel E. Kazin,*[a] Mikhail A. Zykin,[a] Andrey K. Dyakonov,[a] Alexander V. Vasiliev,[a] Maxim A. Karpov,[a] Evgeny A. Gorbachev,[b] Anastasia E. Sleptsova,[b] Matrin Jansen[c]

[a]Department of Chemistry, Lomonosov Moscow State University, 119991 Moscow, Russia. E-mail: kazin@inorg.chem.msu.ru; Tel: +7 495 9393440

[b]Department of Materials Science, Lomonosov Moscow State University, 119991 Moscow, Russia

[c]Max Planck Institute for Solid State Research, Heisenbergstrasse 1, 70569 Stuttgart, Germany

Supporting information

Experimental

Preparation of samples

The compounds with the general composition $CaY_{1-x}Dy_xAlO_4$, where x = 0, 0.05, 1, (samples **1**, **2**, **3**, respectively) were prepared by solid state synthesis using chemically pure $CaCO_3$, Y_2O_3, Dy_2O_3, and Al_2O_3 as starting materials. The chemicals were ground and mixed in an agate mortar and thermally treated in an electric furnace in air in accord with the following schedule: heating for 2 h to 500 °C and annealing for 3 h, heating for 2 h to 800 °C and annealing for 3 h, heating to 1350 °C and annealing for 9 h, air-quenching. The samples were reground and pressed in pellets. The pellets were put in the furnace, quickly heated in air to 800 °C and annealed for 3 h, heated to 1350 °C for 2.5 h and annealed for 9 h, and finally air-quenched.

Characterization of samples

X-ray diffraction was conducted on a Brucker D8 Advance powder diffractometer in the Bragg-Brentano geometry using CuKα radiation in the 2θ range 10 – 120°. The crystal structure was refined by the Rietveld method using the Jana 2006 computer program. The peak's profile parameters, unit cell parameters, positional and isotropic atomic displacement parameters were refined.

Magnetic measurements were performed using a piece of a ceramic sample firmly fixed to a sample holder in a measurement device. ac susceptibility was measured on a Quantum Design PPMS-9 magnetometer in the temperature range of 2 – 30 K in the ac field frequency range of 10 – 10000 Hz and the ac field amplitude of 1 – 5 Oe under magnetic fields of up to 20 kOe. In cases when the $\chi''(f)$ peak position was below 10 Hz the additional ac susceptibility measurements were performed using a Quantum Design MPMS-7XL magnetometer in the ac field frequency range of 0.1 – 1420 Hz and the ac field amplitude of 4 Oe. dc magnetization was registered using a Cryogenics SQUID magnetometer in the temperature range of 2 – 300 K under magnetic fields of up to 70 kOe. The sample susceptibility and magnetization were corrected for the magnetization of the sample holder and for the core diamagnetism using Pascal's constants.

The real χ' and imaginary χ'' parts of susceptibility as a function of ac-field frequency (f and $\omega = 2\pi f$) were fitted simultaneously using generalized Debye model:[1]

$$\chi'(\omega) = \chi_S + \frac{(\chi_0 - \chi_s)\left[1 + (\omega\tau)^{1-\alpha}\sin(0.5\alpha\pi)\right]}{1 + 2(\omega\tau)^{1-\alpha}\sin(0.5\alpha\pi) + (\omega\tau)^{2(1-\alpha)}}$$

$$\chi''(\omega) = \frac{(\chi_0 - \chi_s)\,(\omega\tau)^{1-\alpha}\cos(0.5\alpha\pi)}{1 + 2(\omega\tau)^{1-\alpha}\sin(0.5\alpha\pi) + (\omega\tau)^{2(1-\alpha)}}$$

where τ is a relaxation time, χ_0 and χ_s are equilibrium and adiabatic susceptibilities, α is a relaxation time distribution width. The simultaneous fitting helped to reduce correlations between τ, α, and $\chi_0 - \chi_s$, when the $\chi''(f)$ maximum was out of the ac-field frequency region. When the peak of $\chi''(f)$ shifted beyond an experimental higher frequency limit of 10 kHz at elevating the measurement temperature, a value of the slow relaxing susceptibility $\chi_0 - \chi_s$ was estimated from Curie-Weiss equation which parameters were obtained by fitting a set of lower-temperature values of $\chi_0 - \chi_s$, which in turn were obtained by fitting patterns with the $\chi''(f)$ maximum. The estimated value was used as a fixed parameter in the $\chi_{ac}(f)$ fitting. Such a procedure helped to further decrease correlations and increase reliability of the data. The reliability of this approach we checked by fitting the data with the fully developed $\chi''(f)$ peak: fitting of only lower-frequency part of the curve without the peak and comparing the results with the fitting of the full curve. The obtained both ways values of τ overlapped within one-two standard deviations. The more detailed description on the measurements and the data treatment can be found in ref. [2]. To increase accuracy of the fitting of low and noisy ac susceptibility values measured under fields of 7 kOe and above, a value of χ_0 was determined independently from dc-susceptibility measurements as a differential susceptibility and was fixed during the $\chi_{ac}(f)$ fitting.

The semiempirical calculations of the electronic structure of Dy^{3+} in the $CaY_{1-x}Dy_xAlO_4$ host were performed using the CONCORD program (later version of CONDON)[4] and PHI program[5]. In the CONCORD program, using the experimentally determined coordinates of oxygen atoms in the coordination sphere of Dy^{3+} and varying a partial charge on the oxygen atoms in a point charge model, CF parameters were calculated. The electronic structure was calculated using the full set of microstates for $4f^9$ configuration (2002 microstates). A fair consistency of Kramer's doublet energies with the values of U_{eff} experimentally estimated from ac-susceptibility was obtained for an oxygen partial charge of 0.7e. The oxygen atoms can be considered as constituents of the AlO_4^{5-} anion and the partial charge value is well comparable to the estimated earlier values of 0.46e for an oxygen atom in the PO_4^{3-} group and of 0.91e for intra-channel O^{2-} in the apatite structure.[6] In the PHI program, the electronic structure including electron transition probabilities was calculated within microstates of the ^6H term, and values of powder average magnetization and susceptibility were calculated using microstates of the $^6H_{15/2}$ term and taking into account an inter-ion interaction. The energies of Kramer's doublets calculated using CONCORD or PHI differed by a few cm^{-1} only.

X-ray powder diffraction data

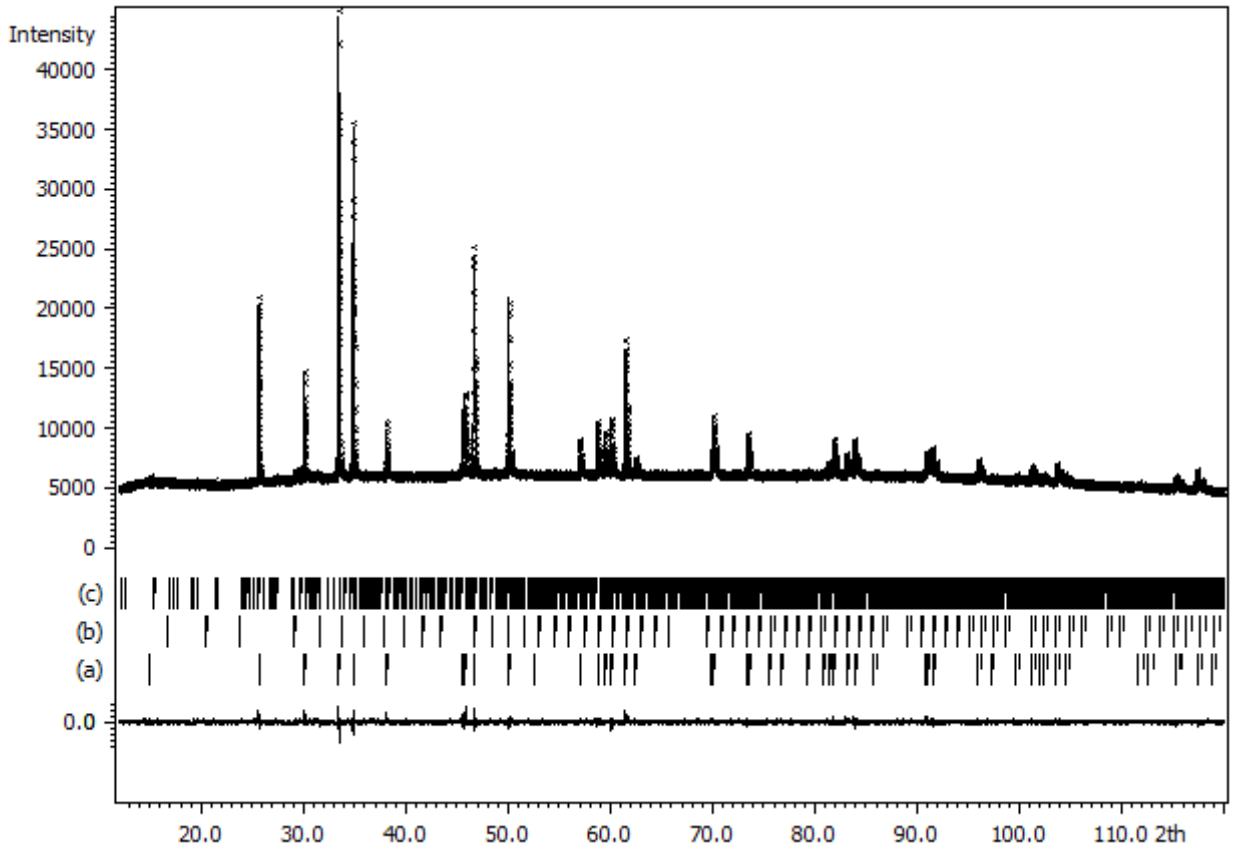

Figure S1. Powder X-ray diffraction pattern of $CaDyAlO_4$. Observed (crosses), calculated (solid line) and difference (solid line below) plots. Positions of Bragg reflections are shown as strokes underneath. (a) the main phase; (b) Dy_2O_3, 0.6 wt. %; (c) $Dy_4Al_2O_9$, 1.6 wt. %.

Table S1. Crystal structure refinement data for $CaDyAlO_4$.[a)]

Temperature (K)	293 K
Wavelength (Å)	1.54187
Space group	I4/mmm
a (Å)	3.6501(1)
c (Å)	11.909(1)
V (Å^3)	158.666(16)
Z	2
2θ range (deg.)	12 – 120
R_{wp}	0.017
R_{all}	0.021
ΔF_{max}, ΔF_{min} (e Å^{-3})	0.99, -1.1

[a)]Further details of the crystal structure investigations may be obtained from the Fachinformationszentrum Karlsruhe, 76344 Eggenstein-Leopoldshafen, Germany (Fax: +49-7247-808-666; E-Mail: crysdata@fizkarlsruhe.de, http://www.fiz-karlsruhe.de/request for deposited data.html) on quoting the depository number CSD 2179057.

Table S2. Atomic parameters and thermal displacement parameters (Å^2) for $CaDyAlO_4$.

Atom	Ca	Dy	Al	O1	O2
Site	4e	4e	2a	4c	4e
SOF	0.5	0.5	1	1	1
x	0	0	0	0	0
y	0	0	0	0.5	0
z	0.35838(7)	0.35838(7)	0	0	0.1684(4)
U_{iso}	0.0080(6)	0.0080(6)	0.0093(12)	0.0126(19)	0.0112(16)

Table S3. Selected interatomic distances (Å) in the crystal structure of $CaDyAlO_4$.

Ca,Dy-O2	2.263(2)	
Ca,Dy-O1	2.4851(3)	4x
Ca,Dy-O2	2.6006(3)	4x
Al-O1	1.82506(1)	4x
Al-O2	2.006(4)	2x

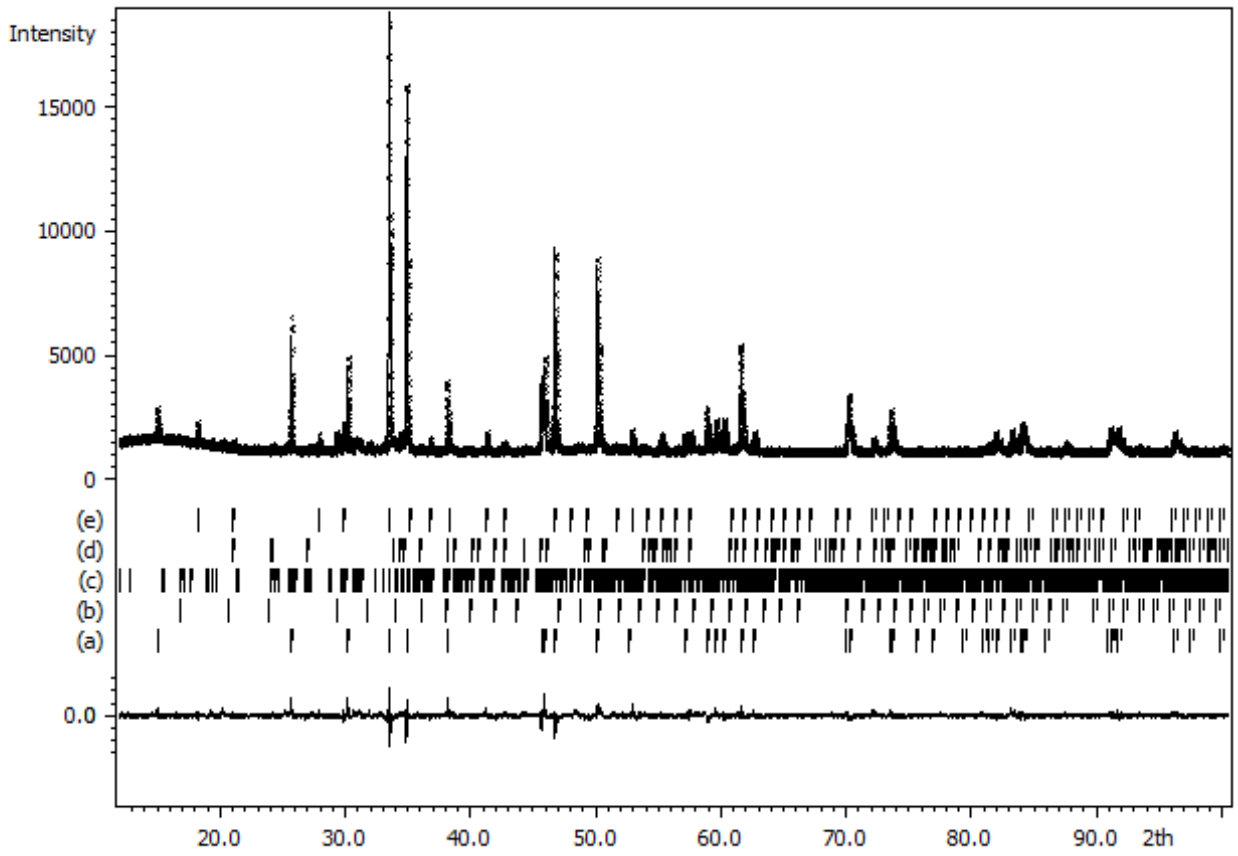

Figure S2. Powder X-ray diffraction pattern of $CaY_{0.95}Dy_{0.05}AlO_4$. Observed (crosses), calculated (solid line) and difference (solid line below) plots. Positions of Bragg reflections are shown as strokes underneath. (a) the main phase; (b) Y_2O_3, 1.9 wt. %; (c) $Y_4Al_2O_9$, 2.8 wt. %; (d) $YAlO_3$, 2.7 wt. %; (e) $Y_3Al_5O_{12}$ 7.9 wt. %.

Table S4. Crystal structure refinement data for $CaY_{0.95}Dy_{0.05}AlO_4$.

Temperature (K)	293 K
Wavelength (Å)	1.54187
Space group	I4/mmm
a (Å)	3.6456(1)
c (Å)	11.883(1)
V (Å^3)	157.930(16)
Z	2
2θ range (deg.)	12 – 120
R_{wp}	0.046
R_{all}	0.043
ΔF_{max}, ΔF_{min} (e Å^{-3})	1.1, -0.95

Table S5. Atomic parameters and thermal displacement parameters (Å^2) for $CaY_{0.95}Dy_{0.05}AlO_4$.

Atom	Ca	$Y_{0.95}Dy_{0.05}$	Al	O1	O2
Site	4e	4e	2a	4c	4e
SOF	0.5	0.5	1	1	1
x	0	0	0	0	0
y	0	0	0	0.5	0
z	0.35866(16)	0.35866(16)	0	0	0.1677(6)
U_{iso}	0.0077(8)	0.0077(8)	0.007(2)	0.008(3)	0.012(3)

Table S6. Selected interatomic distances (Å) in the crystal structure of $CaY_{0.95}Dy_{0.05}AlO_4$.

Ca,Y,Dy-O2	2.270(8)	
Ca,Y,Dy-O1	2.4786(13)	4x
Ca,Y,Dy-O2	2.5967(9)	4x
Al-O1	1.82278(7)	4x
Al-O2	1.992(8)	2x

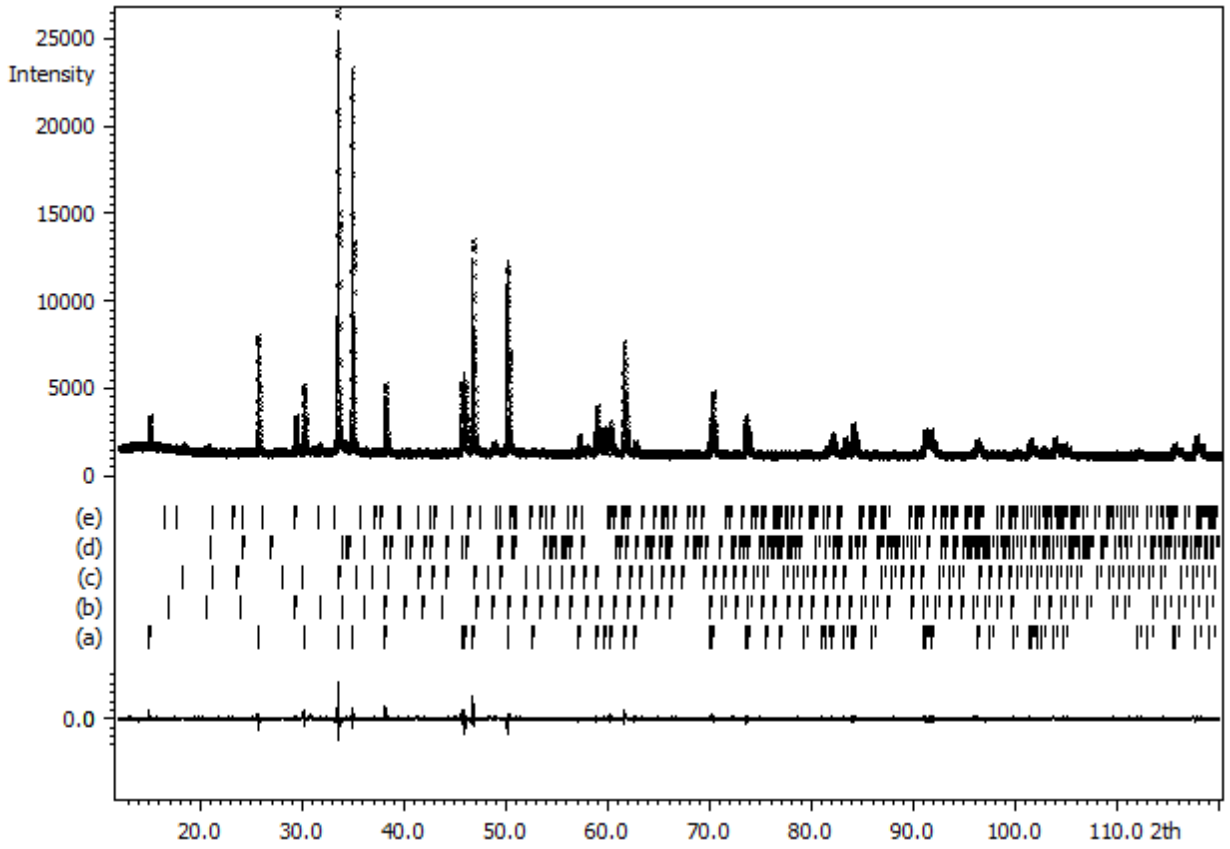

Figure S3. Powder X-ray diffraction pattern of $CaYAlO_4$. Observed (crosses), calculated (solid line) and difference (solid line below) plots. Positions of Bragg reflections are shown as strokes underneath. (a) the main phase; (b) Y_2O_3, 3 wt. %; (c) $Ca_{12}Al_{14}O_{33}$, 1.1 wt. %; (d) $YAlO_3$, 1 wt. %; (e) $CaYAl_3O_7$, 1.3 wt. %.

Table S7. Crystal structure refinement data for $CaYAlO_4$.

Temperature (K)	293 K
Wavelength (Å)	1.54187
Space group	I4/mmm
a (Å)	3.6451(1)
c (Å)	11.884(1)
V (Å^3)	157.900(16)
Z	2
2θ range (deg.)	12 – 120
R_{wp}	0.035
R_{all}	0.018
ΔF_{max}, ΔF_{min} (e Å^{-3})	0.35, -0.44

Table S8. Atomic parameters and thermal displacement parameters (Å^2) for $CaYAlO_4$.

Atom	Ca	Y	Al	O1	O2
Site	4e	4e	2a	4c	4e
SOF	0.5	0.5	1	1	1
x	0	0	0	0	0
y	0	0	0	0.5	0
z	0.35824(7)	0.35824(7)	0	0	0.1684(3)
U_{iso}	0.0072(6)	0.0072(6)	0.0066(9)	0.0087(14)	0.0168(13)

Table S9. Selected interatomic distances (Å) in the crystal structure of $CaYAlO_4$.

Ca,Y-O2	2.2556(16)	
Ca,Y-O1	2.4819(3)	4x
Ca,Y-O2	2.5969(2)	4x
Al-O1	1.82257(2)	4x
Al-O2	2.0018(16)	2x

ac susceptibility data

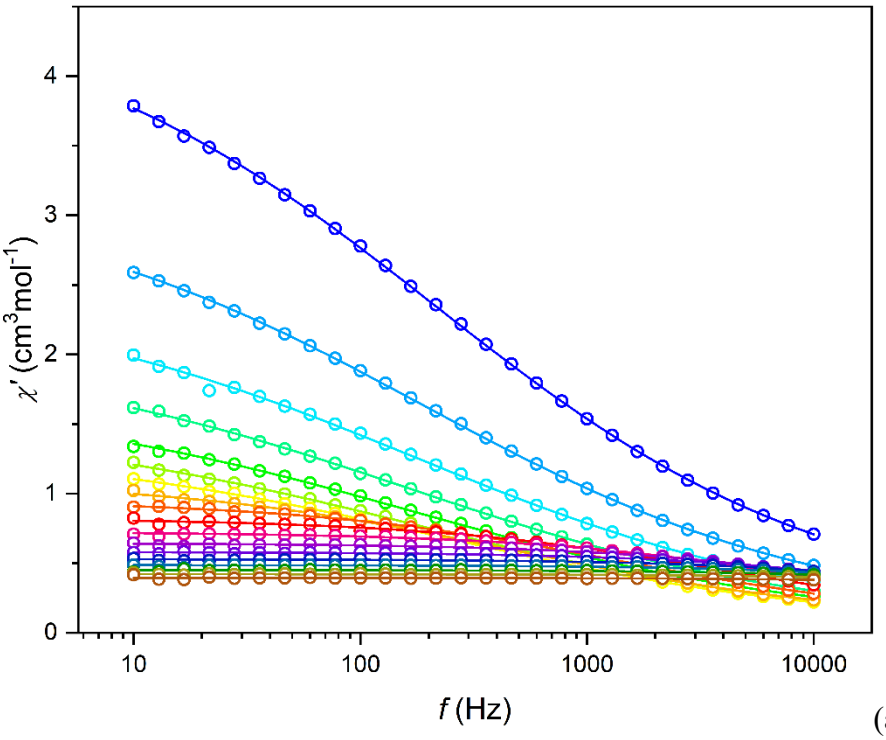

(a)

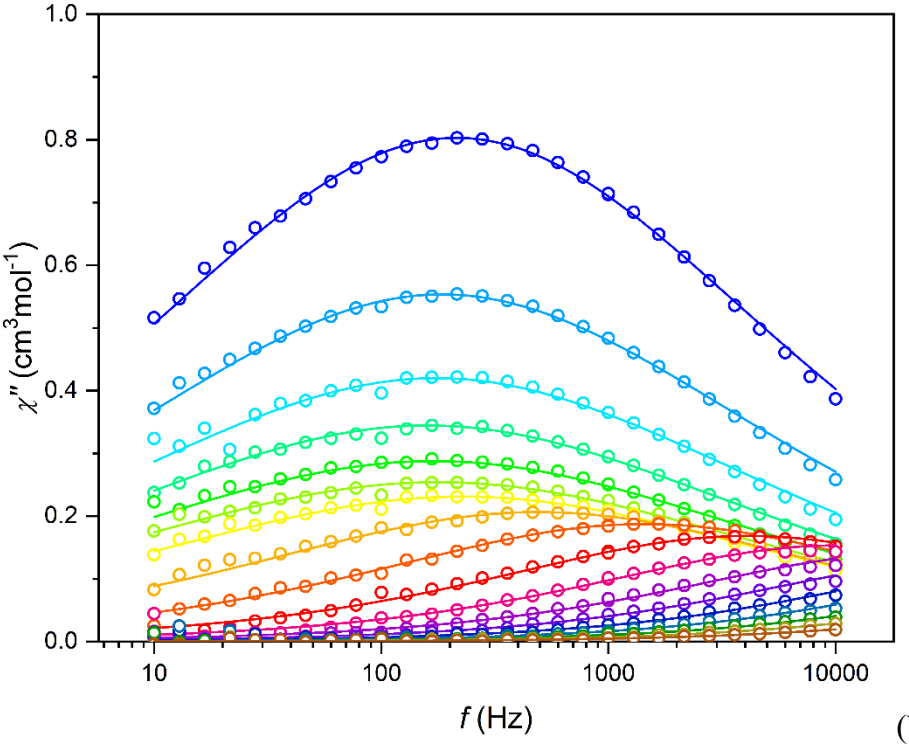

(b)

Figure S4. Frequency dependence of ac susceptibility per mol of Dy for $CaY_{0.95}Dy_{0.05}AlO_4$ at different temperatures under a zero dc magnetic field. (a) – in-phase susceptibility χ', (b) – out-of-phase susceptibility χ''. Symbols – experimental points, lines – fitting. The color codes: from blue to yellow – T = 2 – 8 K, step 1 K; from gold to brown – T = 10 – 30 K, step 2 K.

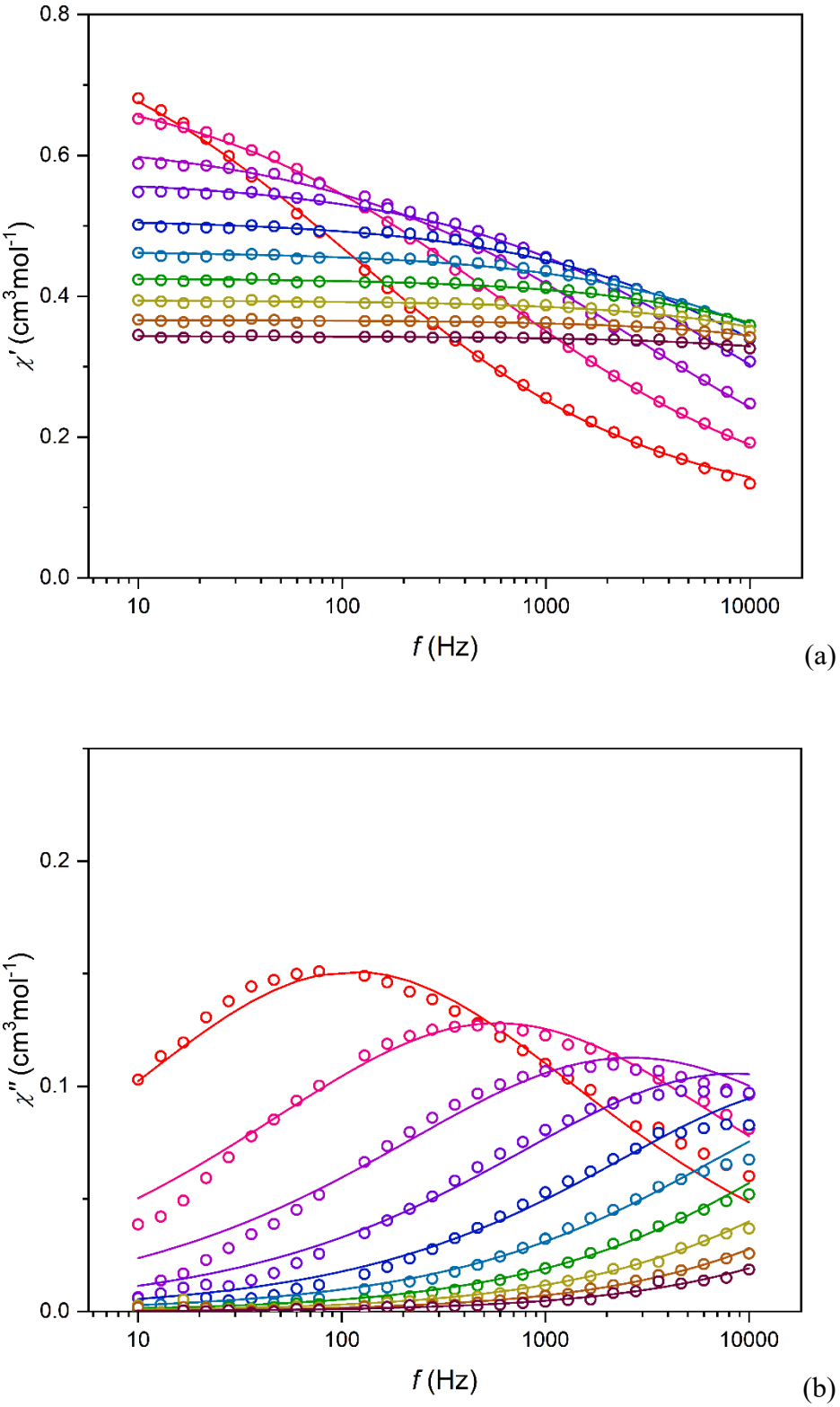

Figure S5. Frequency dependence of ac susceptibility per mol of Dy for $CaY_{0.95}Dy_{0.05}AlO_4$ at different temperatures under a dc magnetic field of 4kOe. (a) – in-phase susceptibility χ', (b) – out-of-phase susceptibility χ''. Symbols – experimental points, lines – fitting. The color codes: from red to wine – T = 12 – 30 K, step 2 K.

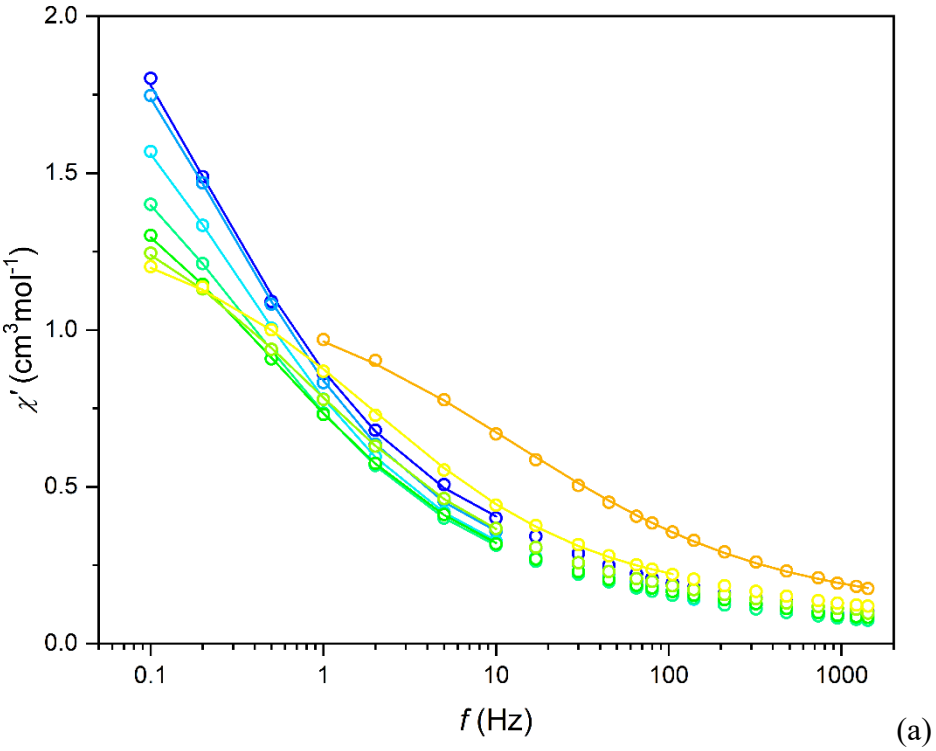

(a)

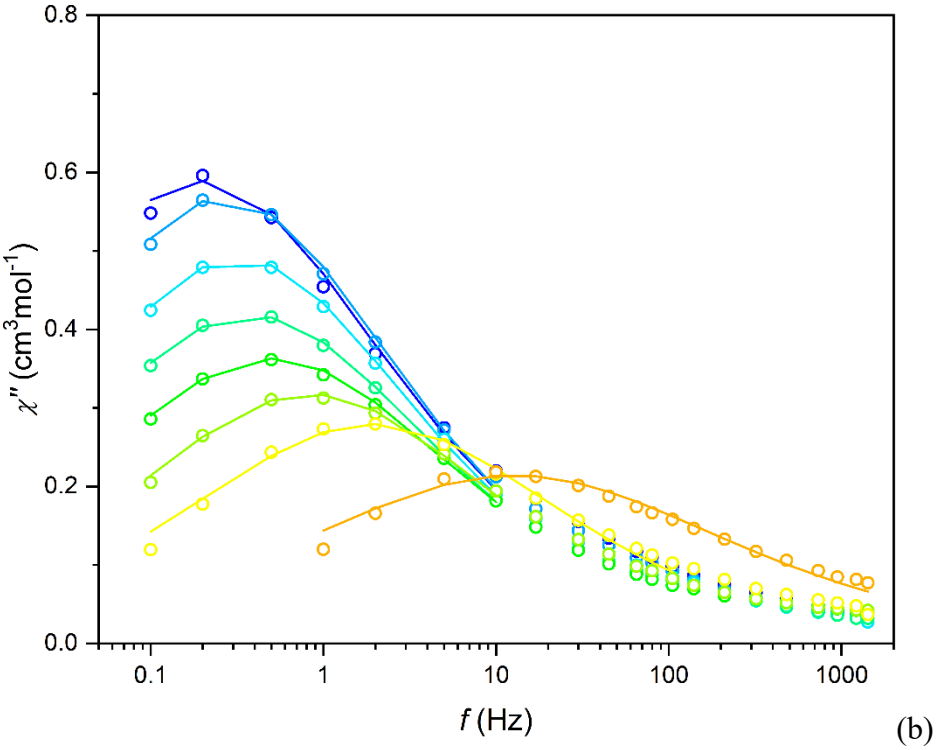

(b)

Figure S6. Frequency dependence of ac susceptibility per mol of Dy for $CaY_{0.95}Dy_{0.05}AlO_4$ at different temperatures under a dc magnetic field of 4kOe. (a) – in-phase susceptibility χ', (b) – out-of-phase susceptibility χ''. Symbols – experimental points, lines – fitting. The color codes: from blue to orange – T = 2, 3, 4, 5, 6, 7, 8, 10 K.

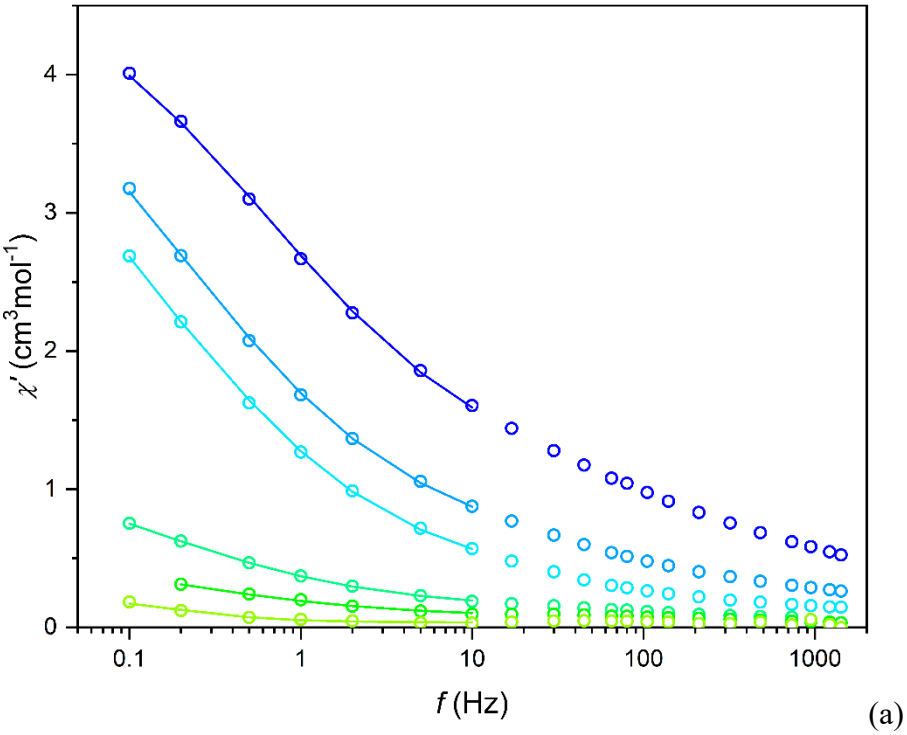

(a)

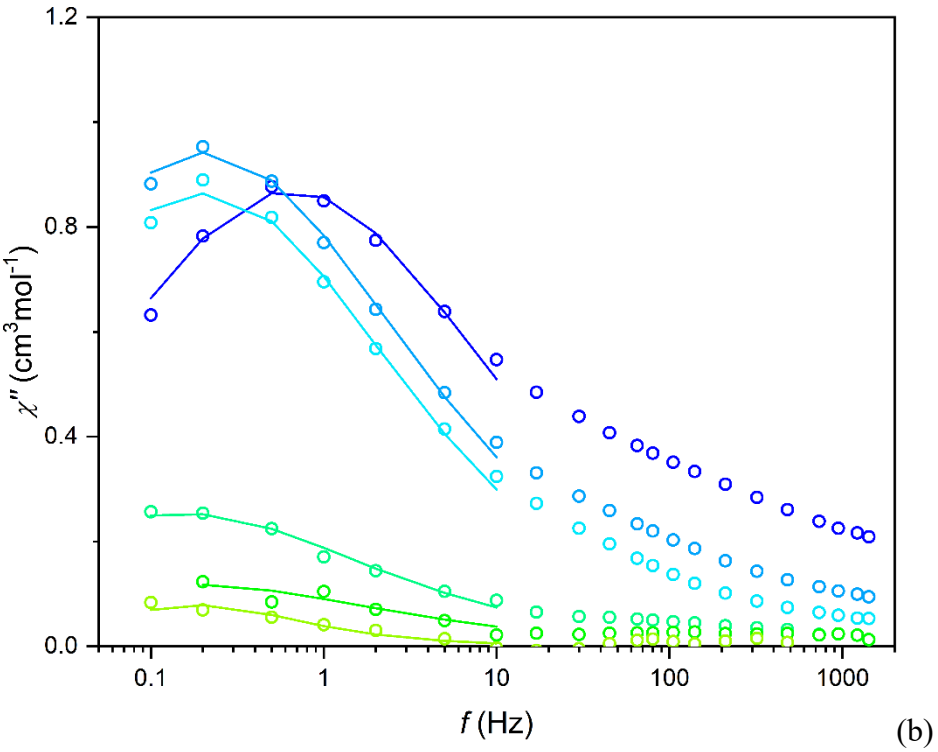

(b)

Figure S7. Frequency dependence of ac susceptibility per mol of Dy for $CaY_{0.95}Dy_{0.05}AlO_4$ under different dc magnetic fields at $T = 2$ K. (a) – in-phase susceptibility χ', (b) – out-of-phase susceptibility χ''. Symbols – experimental points, lines – fitting. The color codes: from blue to yellow – $H = 0.5$, 1, 2, 7, 10, 15 kOe. Plots for $H = 0$ and 4 kOe are shown in Figs. S4 and S6.

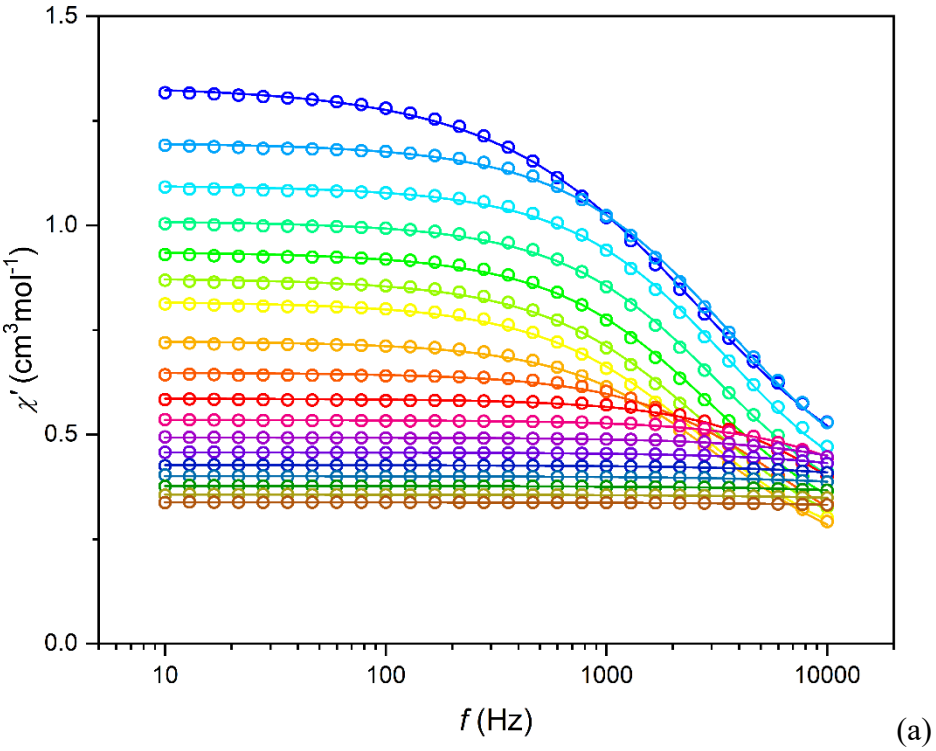

(a)

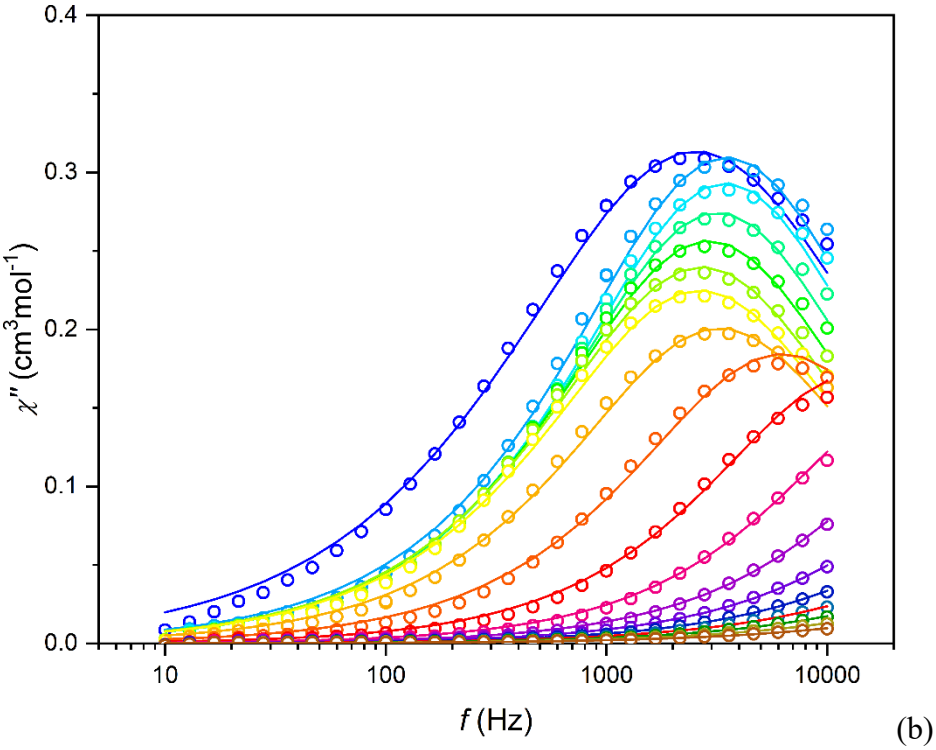

(b)

Figure S8. Frequency dependence of ac susceptibility per mol of Dy for $CaYDyAlO_4$ at different temperatures under a zero dc magnetic field. (a) – in-phase susceptibility χ', (b) – out-of-phase susceptibility χ''. Symbols – experimental points, lines – fitting. The color codes: from blue to yellow – T = 2 – 8 K, step 1 K; from gold to brown – T = 10 – 30 K, step 2 K.

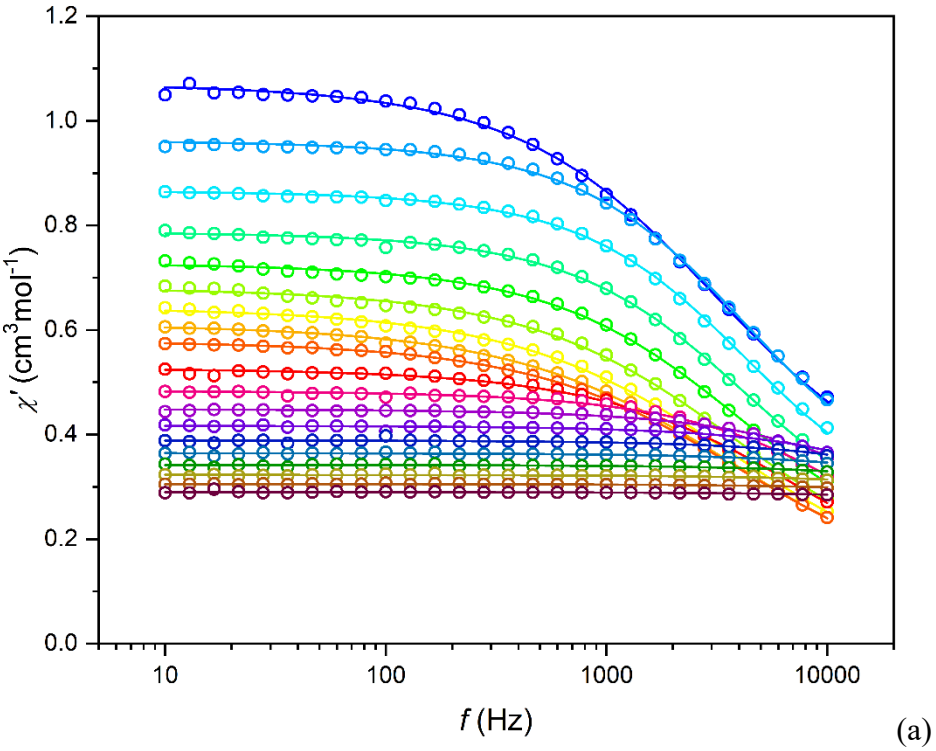

(a)

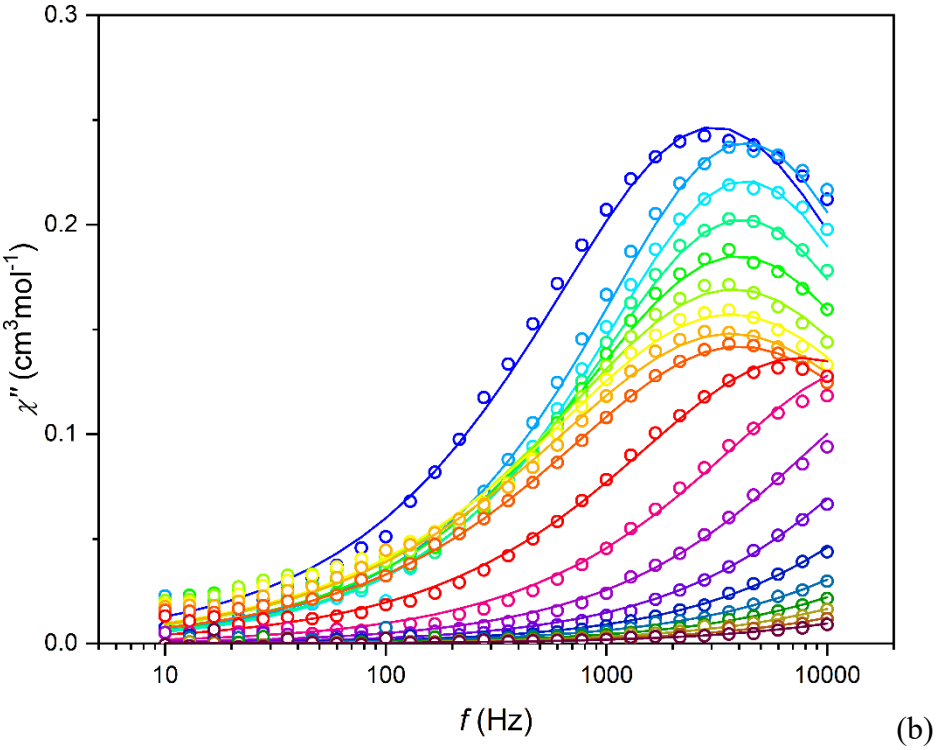

(b)

Figure S9. Frequency dependence of ac susceptibility per mol of Dy for $CaDyAlO_4$ at different temperatures under a dc magnetic field of 4kOe. (a) – in-phase susceptibility χ', (b) – out-of-phase susceptibility χ''. Symbols – experimental points, lines – fitting. The color codes: from blue to orange – T = 2 – 10 K, step 1 K; from red to wine – T = 12 – 30 K, step 2 K.

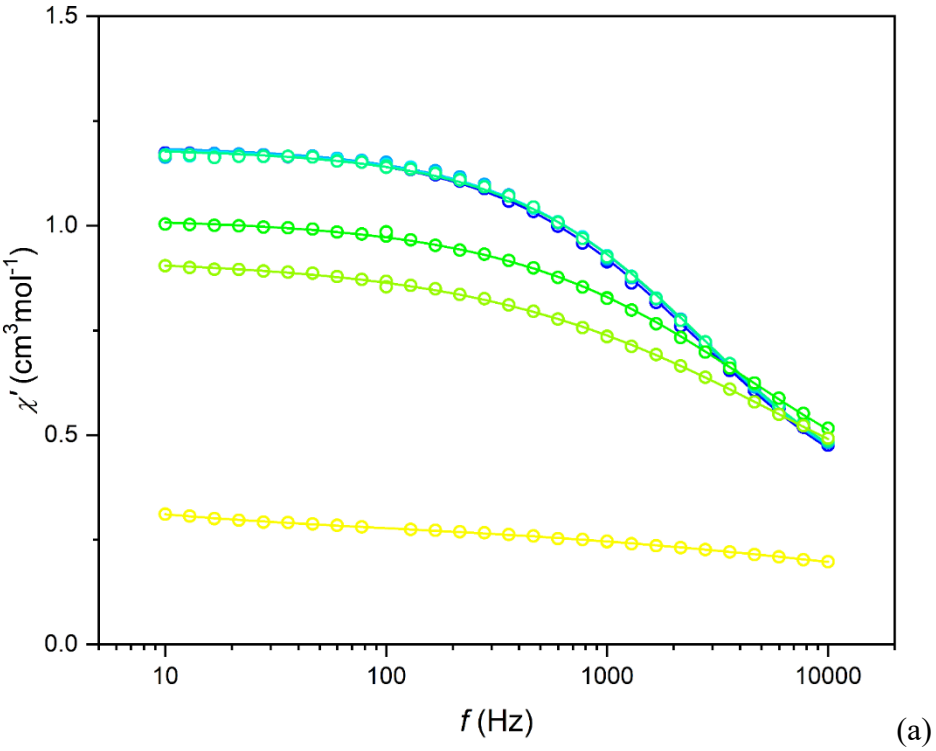

(a)

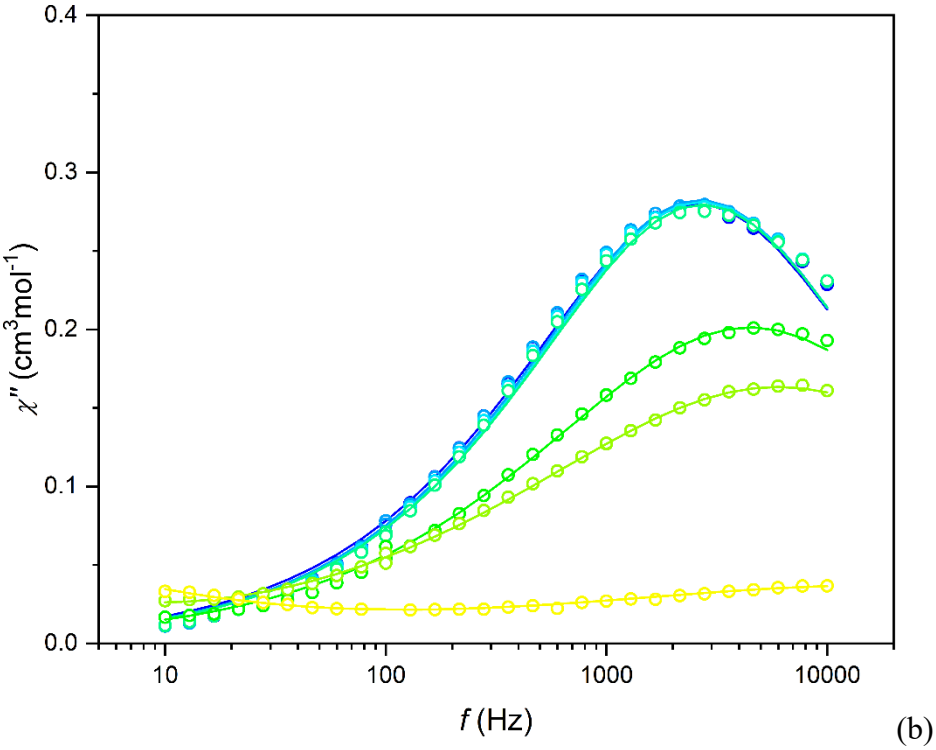

(b)

Figure S10. Frequency dependence of ac susceptibility per mol of Dy for $CaDyAlO_4$ under different dc magnetic fields at $T = 2$ K. (a) – in-phase susceptibility χ', (b) – out-of-phase susceptibility χ''. Symbols – experimental points, lines – fitting. The color codes: from blue to yellow – $H = 0.5$, 1, 1.5, 2, 8, 10, 20 kOe. Plots for $H = 0$ and 4 kOe are shown in Figs. S7 and S8.

Electronic structure data

Table S10. Crystal field parameters in Wybourne notation derived in the program CONCORD for Dy^{3+} using experimental atomic coordinates of the coordination polyhedron (from Table S2). A partial charge on the oxygen atom is 0.7e.

Parameter	Value (cm^{-1})
B_{20}	460.828
B_{22}	0
B_{40}	86.543
B_{42}	0
B_{43}	0
B_{44}	-91.885
B_{60}	16.707
B_{62}	0
B_{63}	0
B_{64}	39.231
B_{66}	0

Table S11. Modeling of the Dy^{3+} electronic structure with the PHI program using crystal field parameters listed in Table S10. The Kramer's doublet energies of the ground term $^6H_{15/2}$ are shown only.

Energy (cm^{-1})	M_J (%)
0	15/2 (99.92)
71.64	13/2 (99.66)
130.0	11/2 (99.18)
174.3	9/2 (98.04)
206.0	+7/2 (95.74), -1/2 (3.79)
225.4	+5/2 (75.33), +3/2 (1.28), -3/2 (17.31), -5/2 (5.60)
246.1	+3/2 (80.34), -5/2 (18.68)
250.1	+1/2 (94.38), -7/2 (4.04)

Analysis of the Dy^{3+} coordination polyhedron geometry with the SHAPE software

Table S12.

```
-------------------------------------------------------------------------------

S H A P E   v2.1         Continuous Shape Measures calculation
(c) 2013  Electronic Structure Group, Universitat de Barcelona
                  Contact:  llunell@ub.edu
-------------------------------------------------------------------------------

CaDyAlO4

EP-9            1 D9h   Enneagon
OPY-9           2 C8v   Octagonal pyramid
HBPY-9          3 D7h   Heptagonal bipyramid
JTC-9           4 C3v   Johnson triangular cupola J3
JCCU-9          5 C4v   Capped cube J8
CCU-9           6 C4v   Spherical-relaxed capped cube
JCSAPR-9        7 C4v   Capped square antiprism J10
CSAPR-9         8 C4v   Spherical capped square antiprism
JTCTPR-9        9 D3h   Tricapped trigonal prism J51
TCTPR-9        10 D3h   Spherical tricapped trigonal prism
JTDIC-9        11 C3v   Tridiminished icosahedron J63
HH-9           12 C2v   Hula-hoop
MFF-9          13 Cs    Muffin

Structure [ML9 ]          EP-9        OPY-9       HBPY-9        JTC-9       JCCU-9
CCU-9     JCSAPR-9      CSAPR-9     JTCTPR-9      TCTPR-9      JTDIC-9         HH-9
MFF-9
 CaO9           ,      36.953,      17.840,      22.712,      19.725,      14.241,
11.674,       4.033,       1.492,       5.129,       2.288,      14.429,      14.442,
2.188
```

References

1. S. M. J. Aubin, Z. Sun, L. Pardi, J. Krzystek, K. Folting, L. Brunel, A. L. Rheingold, G. Christou and D. N. Hendricson, *Inorg. Chem*., 1999, **38**, 5329.

2. a) P. E. Kazin, M. A. Zykin, V. V. Utochnikova, O. V. Magdysyuk, A. A. Vasiliev, Y. V. Zubavichus, W. Schnelle, C. Felser and M. Jansen, *Angew. Chem. Int. Ed*., 2017, **56**, 13416; b) P. E. Kazin, M. A. Zykin, L. A. Trusov, A. V. Vasiliev, R. K. Kremer, R. E. Dinnebier and M. Jansen, *RSC Adv.*, 2020, **10**, 37588.

3. Helmut Schilder, PROGRAM CONCORD, Fachhochschule Aachen, 2013.

4. H. Schilder and H. Lueken, *J. Magn. Magn. Mater*., 2004, **281**, 17.

5. N. F. Chilton, R. P. Anderson, L. D. Turner, A. Soncini and K. S. Murray, *J. Comput. Chem*., 2013, **34**, 1164.

6. P. E. Kazin, M. A. Zykin, O. V. Magdysyuk, V. V. Utochnikova, E. A. Gorbachev, R. K. Kremer, W. Schnelle, C. Felser and M. Jansen. *Dalton Trans.,* 2019, **48**, 5299 (in Electronic Supplementary Information).